

## Chapter 2

# Green Multi-homing RF Architectures

**Abubakar Sadiq Hussaini, Issa Elfergani, Ayman Radwan,  
Jonathan Rodriguez, Laurent Dussopt, Alexandre Giry,  
Michael Pelissier, Sami Aissa, Frederic Fraysse and Dany Lenox**

**Abstract** Next generation handsets will need to be energy aware so as to support 5G services, that are likely to be intelligent and bandwidth hungry, as well as support multi-mode operation (LTE, LTE+, HSDPA, 3G, WiFi among others) in Heterogeneous Networking (HetNet) environment. This vision gives way to stringent design requirements on the RF system design that in today's handset is a key consumer of power. This vision provides the impetus for new research lines that will encompass techniques and the implementation of functional entities so as to minimize the carbon footprint in mobile 5G handsets. The performance of the future handset transceiver depends primarily on the performance of antennae and RF circuit designs. The future handset requires the transceiver to operate efficiently and to be reconfigurable. The current chapter and the sequel present a comprehensive study of new hardware components that can provide a flexible and energy efficient multi-standard transceivers architecture, with proof-of-concept validation for specific use-cases including LTE, TETRA and TETRAPOL. This chapter addresses the global transceiver architecture design in next generation handsets and the antenna front end unit, that is bridged to the RF front end with tunable matching network to provide an adaptive response for maximum power transfer.

---

A.S. Hussaini (✉) · I. Elfergani  
Instituto de Telecomunicações, Aveiro, Portugal  
e-mail: ash@av.it.pt

L. Dussopt · A. Giry · M. Pelissier  
CEA-LETI, MINATEC Campus, Grenoble, France

S. Aissa · F. Fraysse · D. Lenox  
CASSIDIAN, Elancourt, France

A. Radwan · J. Rodriguez  
Instituto de Telecomunicações, Campus Universitário de Santiago,  
3810-193 Aveiro, Portugal

## 2.1 Introduction

This book addresses innovative solutions based on cognitive radio and cooperative strategies for future wireless multi-standard mobile devices towards energy saving whilst achieving high data-rates and better quality-of-service. These new technologies will rely on the multi-standard capabilities of handheld terminals to enable the use of the best available radio-access technology (RAT) or cooperative strategy depending on the available access-points and handsets, required data-rates, battery levels, and service costs among other metrics.

The objective of Chaps. 2 and 3 is to investigate flexible multi-standard transceivers at the hardware level and propose innovative technology blocks targeting energy saving as a new design metric, in addition to the traditional criteria of re-configurability, flexibility that are taken as standard in future emerging handsets. In this chapter, we study the design of multi-standard flexible transceiver and wideband miniature antenna along with a matching network to overcome perturbations caused by the hand or other material close to antenna. Whereas in Chap. 3, we tackle the crucial issue of Power Amplifier (PA) design to provide a complete solution for a full radio front end.

The next-generation of multi-mode transceivers needs to handle many standards with different modulation schemes and signal bandwidths. For example, multi-mode Tx performance metrics such as noise figure, linearity, power consumption and among others should be optimum for each bandwidth. This implies severe constraints on the architecture during the design process. The main goal of the first section in this chapter is to define a multi-standard architecture, which is compliant with the targeted standards which include TETRAPOL, TETRA/TEDS and LTE. The architecture is organized in two parts depending on whether the RF signal envelope is varying or constant: for a variable-envelope modulation (TETRA and LTE for instance), a Cartesian (I/Q) transmitter can be used; whilst for constant-envelope modulation (TETRAPOL for instance), a fractional PLL direct modulator with better noise and power consumption is preferred.

The second part of the chapter considers the optimized antenna units and matching circuitry. Modern handheld terminals put severe miniaturization constraints on the antenna in order to manage more space for additional functions, for example the screen, and battery to name a few. We outline the motivation for the miniature notch antenna, which we designed, implemented and characterized performance in the lab. It covers the GSM-900 band, as well as a wide band from 1.7 to 3.6 GHz. The sensitivity of its impedance to the environment was investigated experimentally and theoretically in the case of a metallic plane, user's hand and user's head, showing significant mismatch losses. The large variations in impedance provided the impetus for an adaptive tuning network that can secure maximum power transfer, even under extreme operating conditions.

A tunable matching network was designed for the miniature antenna based on a CLC pi-network topology using switched capacitors integrated in CMOS-SOI technology. The circuit operates over the 1.7–2.7 GHz band. The measurements show good agreement with the simulations. The tunable network was designed

together with a sensing unit based on power detectors measuring the incident and reflected power levels at the input of the matching network. A reasonable accuracy of  $\pm 2$  dB for the reflection coefficients above  $-8$  dB is expected.

Finally, the chapter concludes by analyzing the performance of the TMN-Antenna module. The results show promising performances with significant efficiency improvement (above 25 %) under difficult operating conditions.

## 2.2 Multi-standard RF Architecture

Over the last decades, there has been an evolution in wireless communications towards multifunction and multi-standard mobile terminals. Reducing the number of external components to a minimum is the key when the same mobile terminal has to process several different standards. The growing economic and social impact of mobile telecommunication devices, together with the evolution of protocols and interoperability requirements among different standards for voice and data, is currently driving worldwide research towards the implementation of fully-integrated multi-standard transceivers.

Recently, numerous low-power and low-cost transceivers have been widely applied in our daily life along with the rapid growth of RF IC technology, such as building automation, remote keyless entry, consumer electronics, home automation, voice communication, sensor networks, health monitoring, and medical diagnosis [1–3]. Most of these wireless transceivers work in 433, 868 or 915 MHz license-free industrial, scientific and medical (ISM) frequency bands, but with different modulation schemes and different signal bandwidths [4, 5]. It is apparent that reliance on a single mode transceiver will not do the job. Therefore, to meet different applications using just one transceiver chip, it is necessary to implement a multiband multi-mode transceiver. Considering the stringent cost and power targets, it is necessary to select the lowest-cost CMOS technology and minimize the number of discrete external components.

### 2.2.1 Rx Multi-standard RF Architecture

Private Mobile Radio (PMR) is a field in radio communications systems widely used by, for example, security forces, and fire brigades. New technologies for high data rates are emerging, with very different usage and constraints, so that architectures need to be analyzed in two different parts, namely narrow-band and wide-band systems.

#### 2.2.1.1 Narrow Band PMR

The legacy analogue PMR was used for voice in a walky-talky mode (call direct mode) or trunked mode as in civil cell networks. NBPMR have been standardized,

as APCO P25 [6, 7] in the US, TETRA [8] in the EU and TETRAPOL [9] in France. These standards use digital modulation with the main motivation to secure the transmission. Some low rate digital features are used like short text messages.

These networks are mainly operated in the 400 and 800 MHz bands. Globally speaking, frequency bands are less standardized than for civil networks. Since customer frequency bands are widely spread, different versions of the same products may be needed to address all customers.

For instance, state-of-the-art 400 MHz products need around 50 MHz of bandwidth, grouping the uplink, downlink and direct mode channels. Different terminal bands are defined (380–430, 440–470 MHz) to gather customer needs. It can be said that NBPMR terminals are able to manage a tremendous number of channels to deal with customer frequency versatility.

It is important to note that terminal usage is very different from regular public cell phone networks. For instance, instead of single user to single user communications, group calls are mainly used; many users listen to the same channel, while only one user transmits pressing a push to talk button. This makes terminals operate mainly in RX mode. The official Schengen scenario is 60 % standby, 35 % RX and 5 % TX, but the actual RX/TX ratio is usually high. This is why the optimization of power consumption in RX mode is very important. Direct mode is mainly used when a trunked network is not available.

Narrow Band PMR (NBPMRs) are designed to be compliant with channels used for analogue PMR networks. The typical channel step is 12.5 or 25 kHz and the modulation bandwidth from 6 to 20 kHz. Furthermore, channels can be offset by  $\pm 6.25$  kHz to ease the coexistence of different customer networks.

These narrow channels drive all the PMR architecture, as it requires:

- i. the synthesizer phase noise to be low in adjacent channels with a very low offset;
- ii. high selectivity at adjacent channel, which is very close to centre frequency;
- iii. very small synthesizer steps (at 400 MHz, the minimum step is 64,000 times smaller than signal frequency).

The legacy of analogue networks make interferer levels very high: the typical selectivity to bi-adjacent interferers is 70 dB. The above points i and ii mean that very high quality coefficient components (as  $\Delta f$  is very small) are required for local oscillators and filters.

## Local Oscillator Architecture

To achieve a low phase noise, the Phase Lock Loop (PLL) filter cut-off frequency has to be low compared to the channel step, in order to filter out the noise contribution of the reference (TCXO) and the phase detector at all interferer frequency offsets; hence, the Voltage Control Oscillator (VCO) is a unique contribution. An integer PLL block diagram is shown in Fig. 2.1.

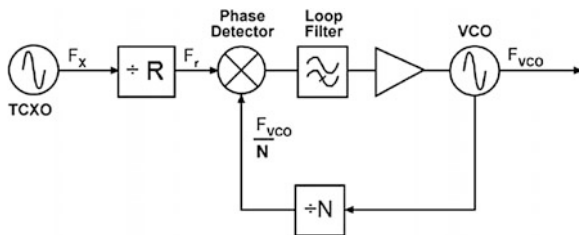


**Fig. 2.1** Integer PLL block diagram

The drawback of the low cut-off frequency is the long settling time of the local oscillator; however nowadays PLL provides speed-up techniques and no rapid change is required for NBPMR due to the narrow channel bandwidth. So settling time is usually not a major issue.

For any architecture, the local oscillator relies on a high-end VCO. Moreover, low phase noise VCO design is a key knowledge to design NBPMR terminals. The required quality factor is so high that, until now, on chip VCO are not able to reach NBPMR requirements.

A common trick to improve the local oscillator phase noise is to design it at four times the required frequency: when the signal frequency is divided by four, the phase noise is improved by 12 dB ( $20 \cdot \log_{10}(4)$ ). This provides good improvements, while high Q can be maintained around 1.5 GHz for the 400 MHz band. For the 800 MHz band, the benefit is less obvious and a balance between the phase noise improvement and the Q value drop has to be studied carefully. A division by two may also be a valid option.

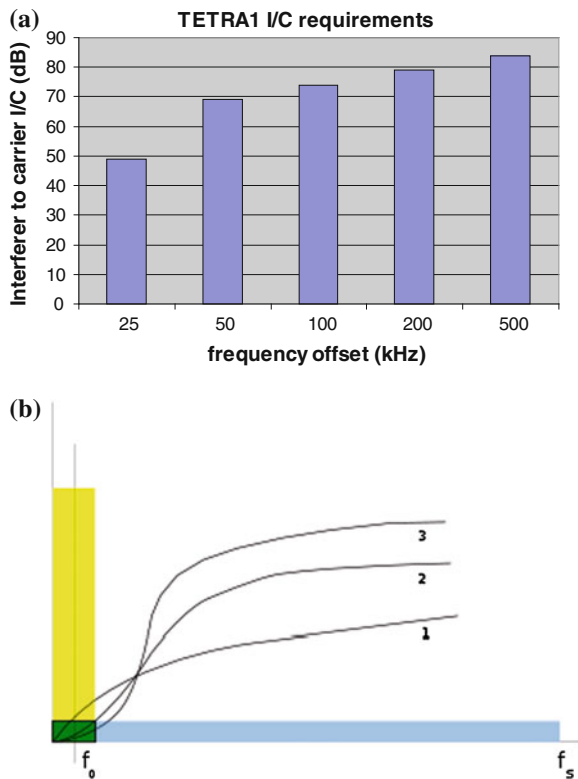
Integer or fractional PLLs can be used: a fractional PLL gives fractional spurious, which may be an issue considering that the typical NBPMR rejection specification is better than 70 dB, whereas an integer PLL needs a comparison frequency equal to the minimum frequency step; this means a high level of phase detector noise, which may be difficult to filter by the PLL loop filter. Eventually, the choice is made according to the PLL phase detector noise and the spurious level.

The typical share of the local oscillator in the RX total power consumption is around 25 %. Considering the harsh phase noise requirements, the design has to be done with discreet components. Only a fine partitioning without over killing specification and an optimized electronic design may reduce the power consumption.

### Analog Versus Digital Filtering Partition

One trend of civil market receivers is to use digital filters. It sounds very attractive, as digital filters can have very high Q, their response is not sensitive to the process or temperature, and their response can be adjusted with filter coefficients without hardware redesign. However, moving filtering functions to the digital domain increases the requirements on Analog to Digital Converter (ADC):

**Fig. 2.2** a TETRA1 I/C from ETSI EN 300-392-2; b  $\Sigma\Delta$  noise shaping



- i. sampling rate has to be increased to sample interferers;
- ii. interferer level increases with the frequency offset. Figure 2.2 shows the Interferer to Carrier ratio (I/C) for adjacent and blocking channels in a TETRA1 system.

Sigma-delta ADCs are a popular architecture for NBPMR: the idea is to oversample the signal and build the output signal using the sum of input signal variations ( $\Sigma\Delta$ ). Sigma delta ADCs can be optimized to shape the output noise out of the useful signal band (green part in Fig. 2.2).

It is clear that a NBPMR leaves room to increase the sampling rate to improve the dynamic range. Furthermore, it eases anti-aliasing filtering. However, it needs down-sampling and corresponding anti-aliasing filtering before delivering the signal to the DSP.

The required ADC dynamic range is the sum in dB of I/C, required C/N for requested BER, headroom for AGC management and a 10 dB margin (as ADC noise is partitioned to be much <RF part). The typical dynamic range for adjacent channel digital filtering only is more than 90 dB in the useful signal bandwidth. But ADC power consumption for this kind of dynamic is very high for handheld devices. Knowing that the ADC power consumption increases linearly with  $\Sigma\Delta$ , oversampling or even increases by 4 each time 1 hardware bit (i.e. 6 dB) is added,

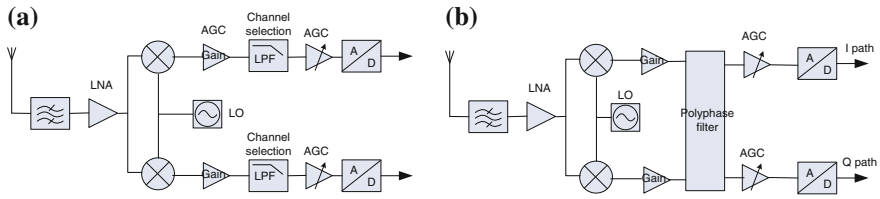


**Fig. 2.3** a TETRA1 I/C from ETSI EN 300-392-2, b “low IF” receiver

bi-adjacent and higher channels cannot be filtered in digital domain. Actually, even a part of the adjacent channels is filtered in the analogue domain to reduce the ADC power consumption in most receivers.

The ADC power consumption, when high dynamic ranges are needed, explains the relatively rare usage of digital filtering in NBPMR terminals.

### Architecture Choice

In both Low-IF and direct-conversion architectures, all receiver filtering functions are performed before the ADC. This means that high dynamic, to handle all interferers, has to be maintained in almost all receiver paths. Also, all constraints are set to base-band filters: high linearity, high attenuation for far jammers, high stability (to maintain adjacent channel filtering without filtering useful signal). This is so challenging that, according to our knowledge, these architectures are not used for NBPMR (Fig. 2.3).

The traditional super-heterodyne architecture is popular for NBPMR. Filtering is usually split between IF using crystal filters technology, baseband and digital domain. The more signal gets through the RX path, the more interferers are filtered and gain may be applied to signal.

Crystal filters are able to reach sufficient quality factors with a centre frequency between 50 and 100 MHz. This makes the first mixer image frequency far enough to be filtered (terminal typical bandwidth is 50 MHz), so that no image rejection mixer is needed. This is a good point since the power consumption increases with the frequency. The crystal filter frequency is too high for sampling, so the signal is converted to a second IF, which may be 0 Hz. Additional filtering may be added at IF2 to reduce the ADC dynamic. Image rejection is often used for the second mixer as the consumption penalty is low and the image frequency close to the useful band (Fig. 2.4).

#### 2.2.1.2 Wide-Band PMR

Giving details about wide band PMR (WBPMR) is difficult as it is still under development. It is designed using civil technologies like LTE for high-speed data transmission. In a wide-band system, many of the NBPMR constraints vanish; for instance, channels are more than 50 times wider so that filtering requirements are lower. Moreover, there is no reason for much more RX operating time than TX.

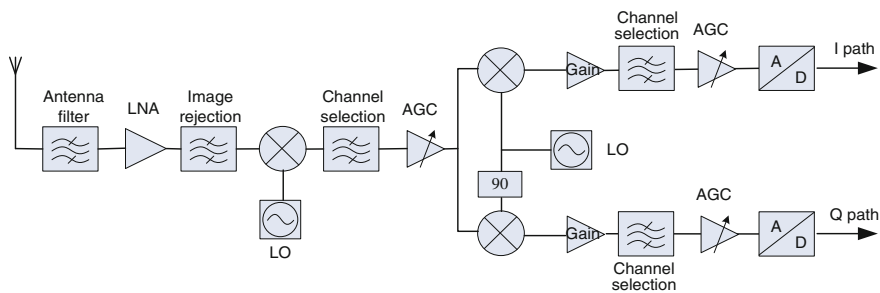


**Fig. 2.4** Super-heterodyne receiver

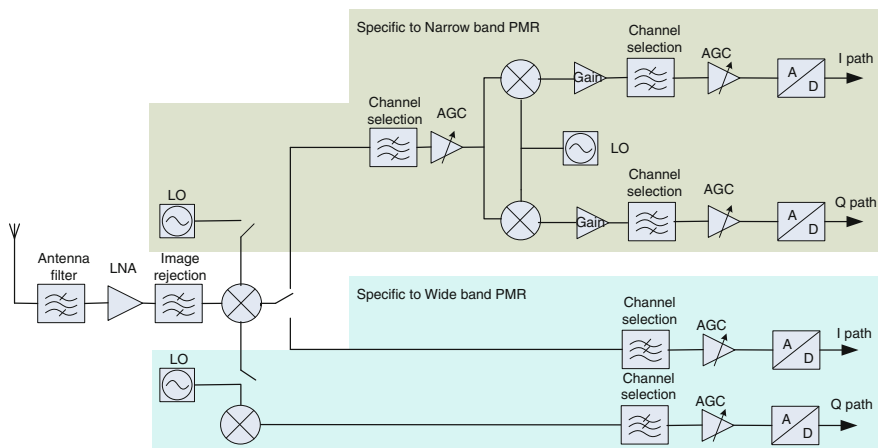


**Fig. 2.5** The foreseen architecture of multi standard receiver

The foreseen architecture is direct conversion as it is popular in civil network devices. As less filtering is required, it can be implemented at baseband only. Modulation width is more than 1 MHz so the impact of  $1/f$  noise is much less than for narrowband PMR. The base band design at  $IF = 0$  Hz is not so challenging.

Faster local oscillator settling time and reasonable phase noise specification make wider PLL loop possible, relaxing VCO specification. It is worth to use several VCOs for wideband operation as narrow-band VCO power consumption is very high (Fig. 2.5).

### 2.2.2 TX Multi-standard RF Architecture

The next-generation of multi-mode transceivers needs to handle many standards with different modulation schemes and signal bandwidths. Multi-mode TX performances such as noise, linearity, power consumption and others should be



optimum for each bandwidth. This implies severe constraints on the architecture to deal with during the design. The main goal of this section is to define a multi-standard TX architecture, which is compliant with the targeted standards which are TETRAPOL, TETRA/TEDS and LTE.

The architecture is organized in two parts depending on whether the RF signal envelope is varying or constant:

- For a variable-envelope modulation (TETRA and LTE for instance), a Cartesian (I/Q) transmitter can be used;
- For a constant-envelope modulation (TETRAPOL for instance), a fractional PLL direct modulator with better noise and power consumption is preferred.

### 2.2.2.1 Cartesian (I/Q) Direct-Up Transmitter

The direct up-converter, also commonly known as homodyne or Zero Intermediate Frequency, is composed of only one frequency conversion stage as shown in Fig. 2.6.

The base-band signals (I and Q), issued from a DSP, are converted to analogue via Digital to Analogue Converters. These signals are then filtered and directly modulated to RF frequency by two mixers driven in quadrature by an RF synthesizer.

The main advantages of this architecture are its simplicity and low number of components making it suitable for a high level of integration. Indeed, as the channel rejection is done dynamically by summing the mixers outputs, there is no need for an external image filter.

Such architecture is attractive for a complex I/Q modulation, but implies hard constraints on the IQ modulator. The IQ modulator is a multiplier providing the transposition to RF frequency. It needs the baseband information components (I and Q), and a carrier RF frequency provided by the RF synthesizer. The design of each component is critical as the noise added by the multipliers will be impossible to filter and can violate the out-of-band spurious emission. A major difficulty in the modulator design is the matching between the I and Q paths. Indeed, gain and phase imbalances create unwanted images (Fig. 2.7).

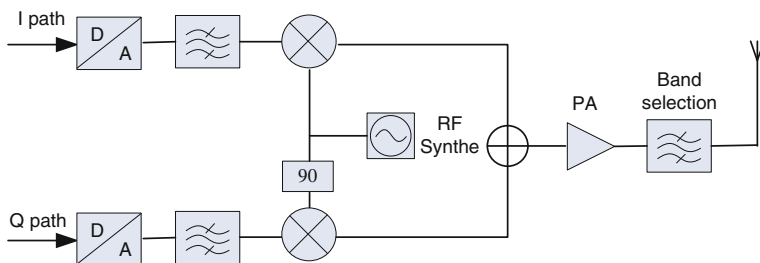
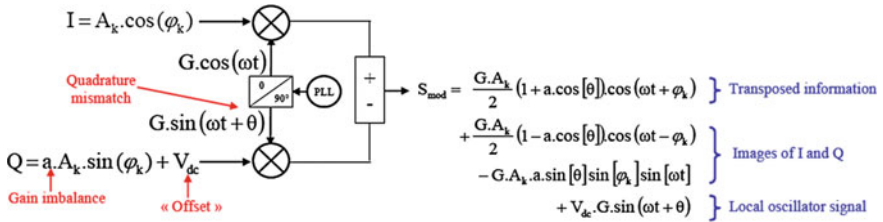


Fig. 2.6 Direct-up transmitter



**Fig. 2.7** Unwanted generated signals

The frequency synthesizer generates the RF signal required for transposition. This RF signal has to be stable with a high resolution to address all channels (the distance between two channels may be as low as 6.25 kHz). Moreover, the local oscillator phase noise should be compliant with the targeted standard performances especially ACLR1 and ACLR2. As a reminder, Adjacent Channel Leakage Ratio (ACLR) is defined as the ratio of the transmitted power to the power in the adjacent radio channel. This figure of merit represents the noise added by the transmitter in the adjacent channels. This noise can disturb the other users present in the same band and the receiver of the base station. The allowed limits are defined by the ACLR specifications. This is the reason that the noise added by local oscillator must not degrade the ACLR level.

After analyzing the targeted standards, it was found that only LTE could use directly this architecture by carefully designing each block. TETRAPOL is too restrictive with respect to wide-band spurious while TETRA would need linearization.

### 2.2.2.2 Cartesian (I/Q) Direct-Up Transmitter with Cartesian Feedback Loop

To be able to address the TETRA standard, a Cartesian Feedback Loop was introduced, as shown in Fig. 2.8.

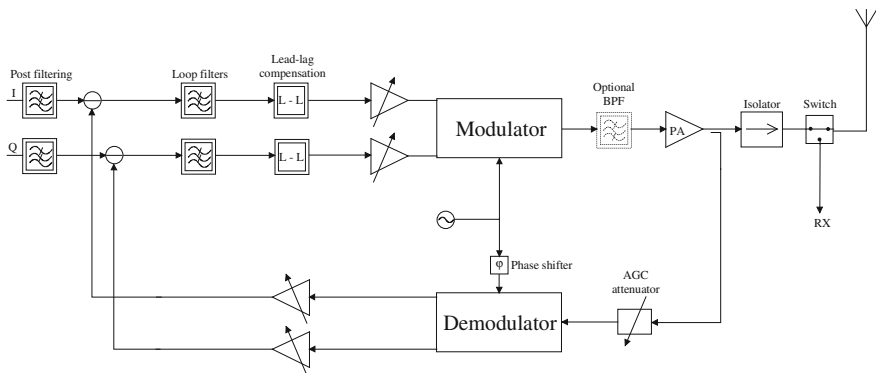


**Fig. 2.8** Cartesian feedback Loop implementation

The information signal is split in I (In phase) and Q (Quadrature) and converted to analogue signal. These signals are compared with the feedback signals, then up-converted to RF frequency and finally summed into a single modulated signal. This modulated signal is then amplified and sent to the antenna. A part of the output signal is down-converted in order to recover I-feedback and Q-feedback signals.

This Cartesian loop helps improving the linearity by reducing the distortion of the circuits in the forward path such as the modulator and the power amplifier.

### 2.2.2.3 PLL for Phase Modulation

The two previous architectures are not suitable for TETRAPOL standard because of the noise generated by the multipliers that makes these solutions non-compliant with the out-of-band spurious emission specification. As TETRAPOL uses a constant signal envelope, another approach is used which consists of indirect modulation of the VCO through the control of the VCO frequency and yields to the simplest transmitter solution of those presented, as shown in Fig. 2.9.

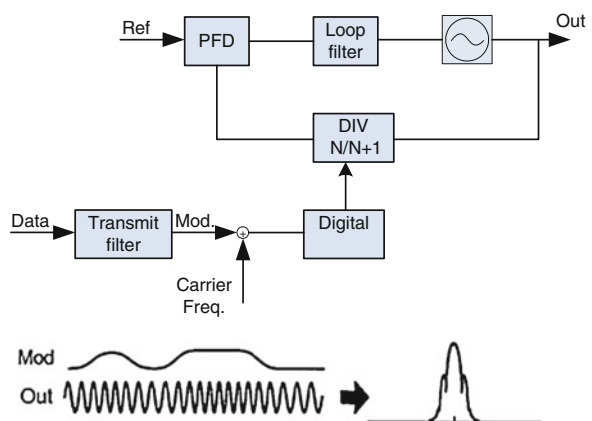
Compared to a direct modulation of the VCO (Fig. 2.10), the D/A converter can be removed and the frequency drift defect during the modulation is eliminated.

The indirect modulator structure depicted in Fig. 2.9 is considered as the optimal topology for frequency or phase modulation. The architecture is composed of two main blocks:

- frequency synthesizer that generates the RF carrier. The frequency resolution must be lower than 1 Hz;
- transmit filter which is necessary to produce an efficient modulation signal.

The digital input data stream, which is first filtered by the transmit filter (FIR), has a Gaussian response. The data are then summed with a nominal value which corresponds to the carrier frequency and fed into a  $\Sigma\Delta$  converter, the output of which controls the instantaneous divide value of the PLL. So, the nominal value set the carrier frequency and the variations correspond to the modulation of the output value by the input data stream.

**Fig. 2.9** Fractional-N modulator (indirect modulation of VCO)



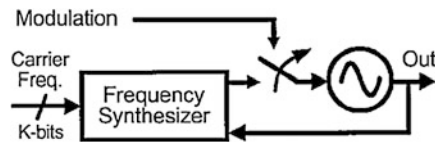


**Fig. 2.10** Direct modulation of VCO

Figure 2.11 illustrates the transient and frequency behavior of such architecture.

The main important aspect is the noise behavior of the loop which has to be optimized in order to reach all the TETRAPOL performances. Figure 2.12 illustrates the results of a noise study in TETRAPOL environment which proves the feasibility of this architecture for TETRAPOL:

- PN\_R4, PN\_R3 and PN\_R2 correspond to the phase noise contribution of the loop filter element;
- PN\_VCO corresponds to the phase noise of the VCO at 400 MHz;
- PN\_SD5 corresponds to the phase noise of the sigma-delta;
- PN\_PFD corresponds to the phase noise of the phase frequency detector;
- PN\_REF corresponds to the phase noise of the crystal reference;
- PN\_total is the sum of all the noise contributors.

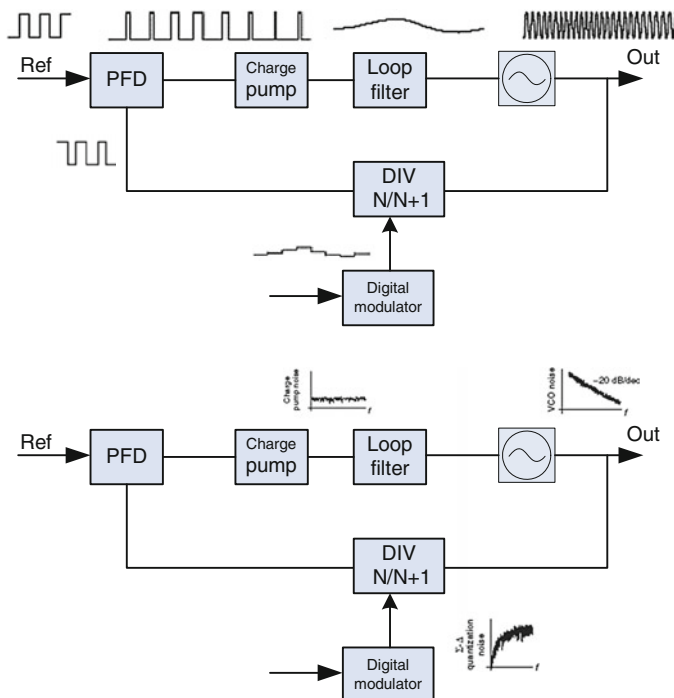


**Fig. 2.11** Transient and frequency behavior

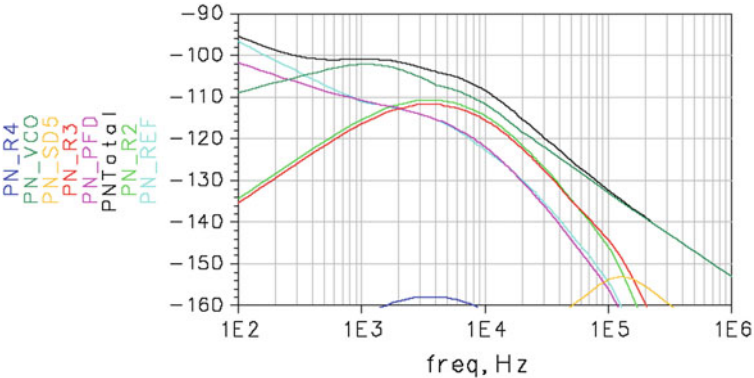


Fig. 2.12 Noise analysis

Generally, the indirect method, which involves the use of a phase locked loop (PLL) has the advantages of low power, feasibility of monolithic implementation, and phase coherence during frequency transitions and has a low phase noise, fine frequency resolution and fast dynamics.

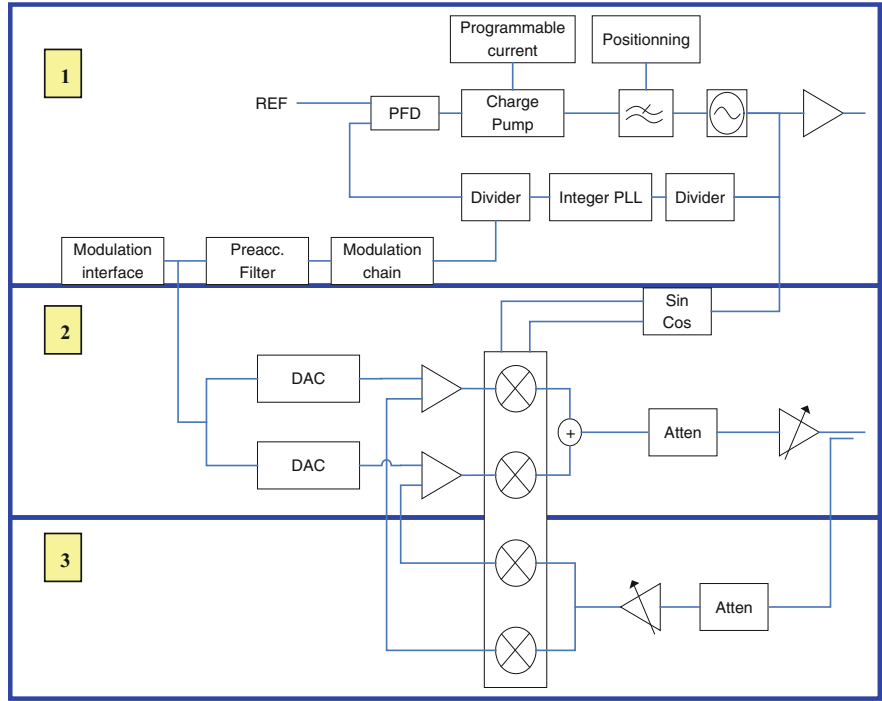


Fig. 2.13 TETRAPOL, TETRA and LTE multi-standard architecture

#### 2.2.2.4 Global TX Multi-standard Architecture

Figure 2.13 illustrates the global TX architecture. In order to save silicon area and power consumption, the TETRAPOL fractional modulator is used as Local Oscillator when TETRA or LTE mode is activated.

In summary, the operation of this architecture is:

- When TETRAPOL mode is activated, only block 1 is ON while others are OFF;
- When LTE mode is activated, block 1 and 2 are ON;
- When TETRA mode is activated, block 1, 2 and 3 are ON.

### 2.3 Tunable Matching Network and Miniature Antenna for Multi-standard Handsets

#### 2.3.1 Miniature Dual-Band Antenna

The rapid expansion of wireless communications demands the use of compact transceivers with multiband operation. This requirement presents a considerable challenge to the antenna designer, who has to deliver a small volume multiband antenna embedded into the transceiver's case. The main electrical features of these antennas are small size and multi-band operation. Cell phones have evolved from former dual-band designs (ex: GSM900 and 1,800 MHz) to more sophisticated designs such as those having GSM (global system for mobile communications, 860–980 MHz), DCS (digital communication system, 1,710–1,880 MHz), PCS (personal communication services, 1,880–1,990 MHz), universal mobile telecommunications system (UMTS, 1.9–2.17 GHz), WiBro (2,300–2,390 MHz), Bluetooth (2,400–2,480 MHz), satellite-digital multimedia broadcasting (S-DMB, 2,630–2,655 MHz), and Worldwide Interoperability for Microwave Access (WiMAX) for IEEE802.16 bands (3.3–3.7 MHz). Many mobile handsets have design constraints on size and weight, partly driven by customer expectations, and partly owing to the increasingly ubiquitous use of location-aware applications. From an antenna design perspective, these constraints may be summarised thus to reduce the antenna size with unchanged, or improved, performance characteristics.

Several antenna size reduction techniques have been proposed over recent decades, including the use of high permittivity substrate, shorting pins, shorting walls, and modification of the geometry of the internal antenna [10–12]. Recently, another size reduction technique has been proposed, using the magnetic wall concept [13–15], the use of fractal geometry [16], employment of ground slots [17–20] and meta-materials technique [21–23].

### 2.3.1.1 Design and Nominal Performances

A miniature notch slot antenna was designed. The antenna is etched on a ground plane of size  $110 \times 50 \text{ mm}^2$ , which is representative of typical current smartphones. A top and side view of the antenna is presented in Fig. 2.14a. The thickness of the PCB is 0.8 mm. The notch antenna is fed through a coupled microstrip line, near its centre, and loaded by a parasitic capacitive load near its short end. The antenna impedance matching is realized through an open stub and an inductive line section at the input, as shown in Fig. 2.14b. More details of the antenna design and optimization can be found in [24].

The antenna exhibits a dual-band response with a lower band at 815–1,010 MHz ( $\text{VSWR} < 3:1$ ) covering the GSM standard (Fig. 2.15). The upper band at 1,840–3,365 MHz ( $\text{VSWR} < 2:1$ ) covers the DCS-1800, IMT-2000, WiFi 802.11b/g/n, and LTE (band 7 and 38) standards. The WiMAX band at 3.4–3.6 GHz is also covered with a  $\text{VSWR} < 3:1$ .

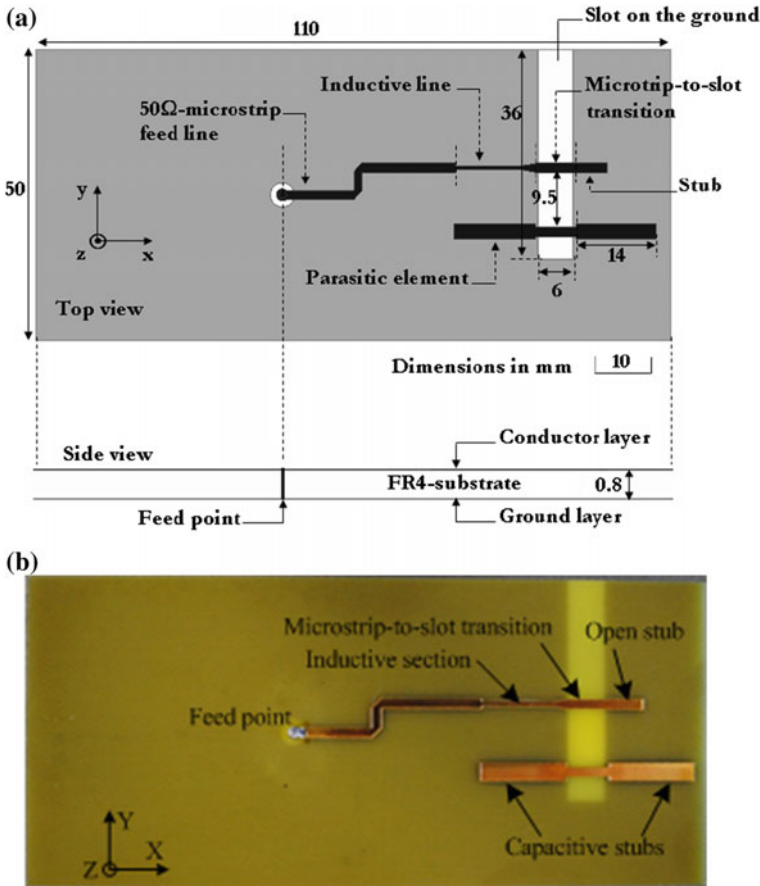
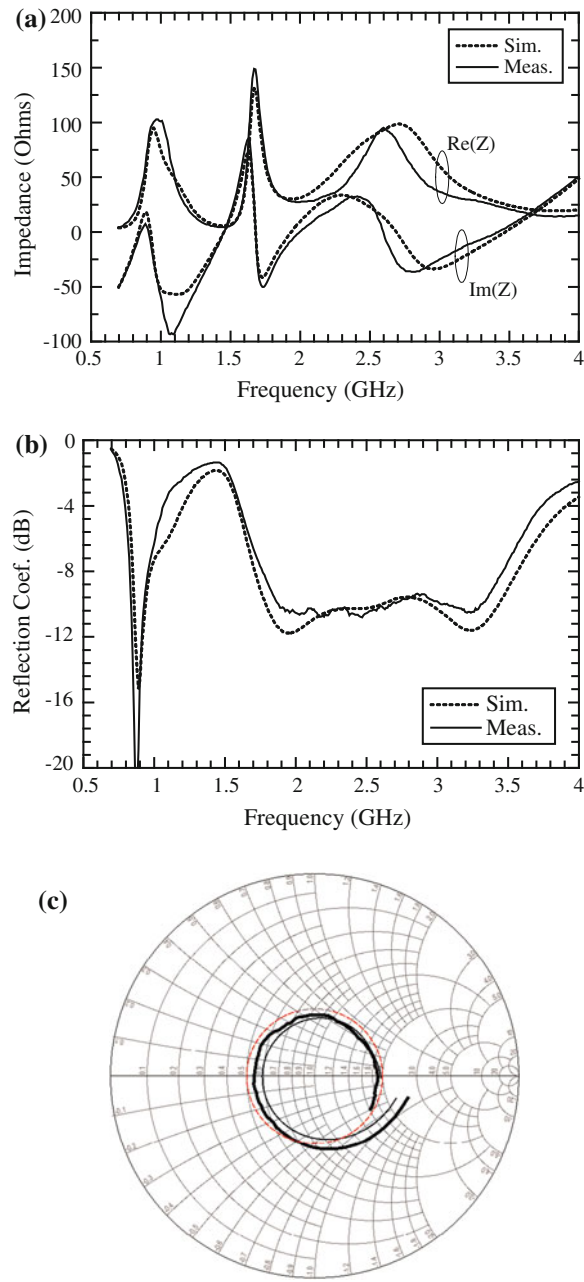


Fig. 2.14 a Top and side view of the antenna; b photograph

**Fig. 2.15** **a** Measured and simulated impedance of the antenna; real and imaginary parts, **b** reflection coefficient and **c** impedance on the Smith chart at 1.7–2.7 GHz



The radiation patterns as well as the antenna gain were measured in an anechoic chamber (Fig. 2.16a, b) and are in good agreement with the simulations. The experimental efficiency of the antenna is above 70 % in each frequency band.



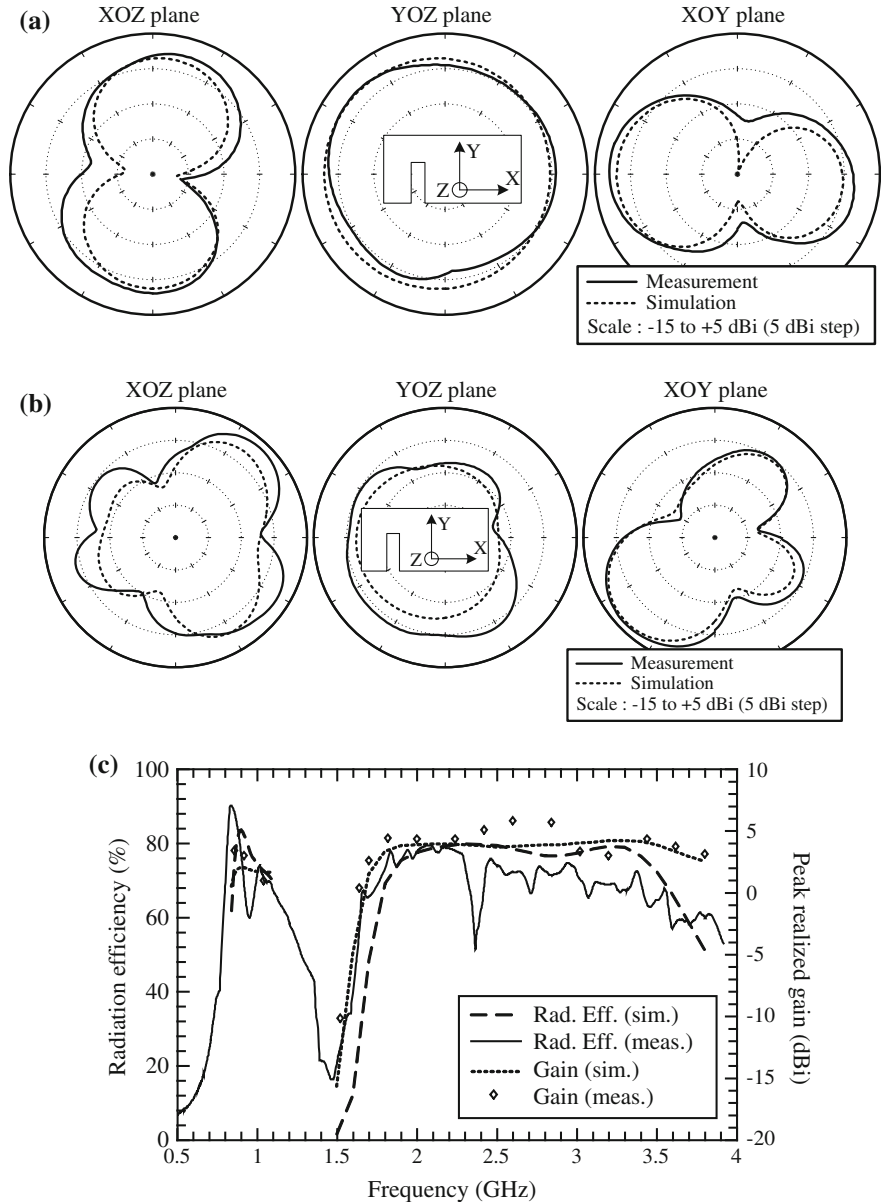


**Fig. 2.16** **a** Measured and simulated radiation performances of the antenna; radiation patterns at 920 MHz, **b** radiation patterns at 1,800 MHz, and **c** gain and radiation efficiency

Overall, the antenna has been fully characterized experimentally and its performance is in very good agreement with the simulations.

### 2.3.1.2 Impedance Sensitivity to the Environment

The most significant perturbation of the antenna occurs in presence of a metallic objects in its close vicinity. We investigated the behavior of the antenna at a varying distance above a metal plane parallel to its ground plane (Fig. 2.17). The simulations and measurements exhibit a fairly good agreement. More specifically, the GSM-900 band is very significantly affected at distances closer than 50 mm. The 1.7–2.1 GHz band is also significantly mismatched at distances lower than 23 mm. In the case of the ISM-2400, LTE and WiMAX bands, the mismatch become critical for distances below 10 mm.

In the normal operation of a hand-held terminal, the user's hand usually impacts the antenna performances. We tested the antenna reflection coefficient in the case of different grips (Fig. 2.18). The exact hand grips are not the topic of discussion here, but rather the perturbation effect they have on the antenna. Most of hand grips do not result in a strong mismatch, i.e. the reflection coefficient remain below  $-6$  dB. In some cases, where a finger is very close to the antenna's slot (Hand grip #2 and #6 in Fig. 2.18), the impact is stronger with reflection coefficients in the range of  $-3$  to  $-5$  dB. The corresponding reflection loss is in the range of 2–3 dB.

This assessment of the hand effect was done experimentally. Although some simulations can be done to get a more complete view of the antenna's performances (radiation pattern, efficiency), it is very difficult to implement a hand EM model close enough to a real hand grip to be able to perform simulation/measurement comparisons.

## 2.3.2 Tunable Matching Network

Matching impedance networks have become ubiquitous in all radio-frequency (RF) transmitters and receivers, especially in wireless mobile devices such as handheld computers (PDs) and cellular phones. Fixed matching networks are inserted between the power amplifier (PA) module and the antenna. The amplifier output impedance has to be matched to the low antenna impedance through an efficient matching network. A well matched RF system is required to increase the reliability and power efficiency of the system. However, antenna input impedance is affected by the presence of surrounding objects [25–28], and can fluctuate significantly with the antenna close to the human body or with the position of the hand on a handset that may bring a mismatch in which can cause more than half of the transmitted power to be reflected [29]. This leads to reduce the radiated power efficiency which in turns increases the demand on the battery.

To deal with this matter, tunable matching networks have been recently proposed [30–33]. Considering the size; matching range; and insertion loss constraints

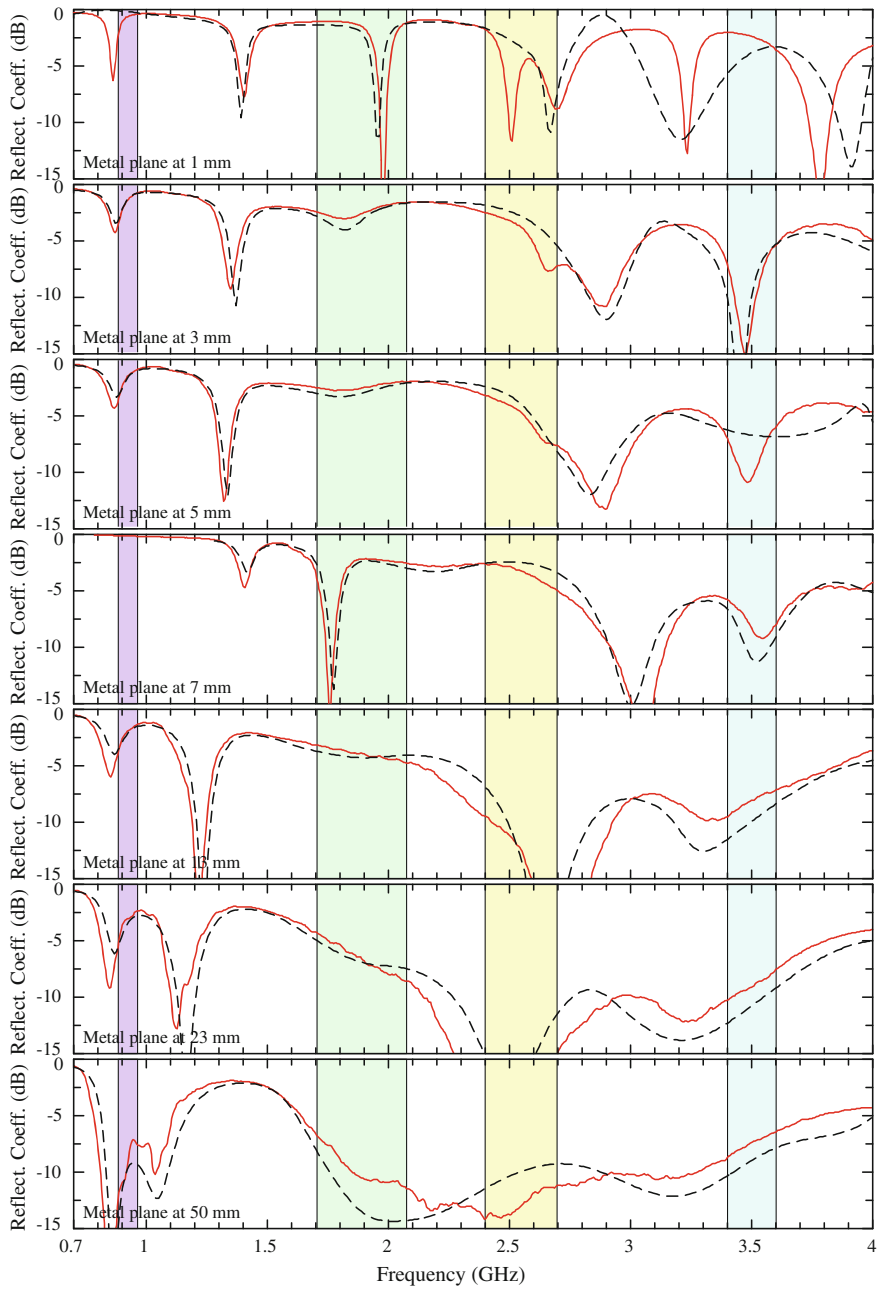
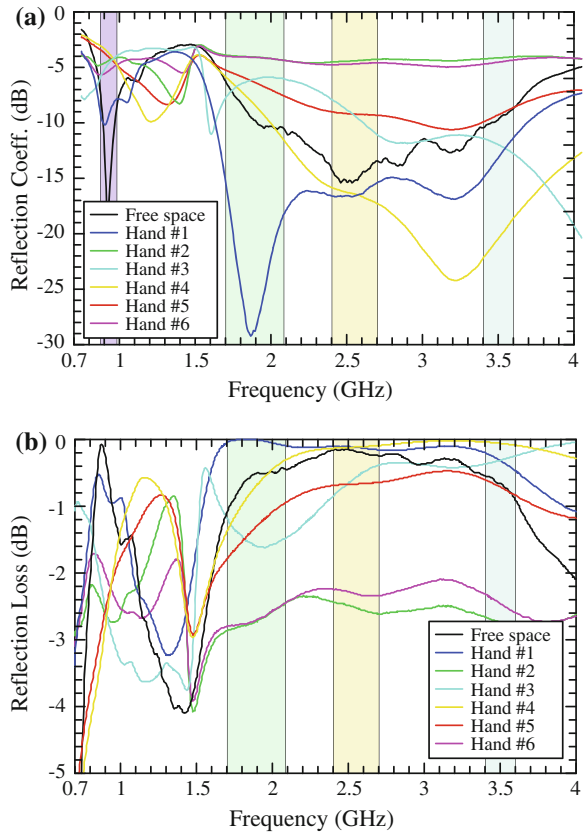


**Fig. 2.17** Measured (*red*) and simulated (*black*) reflection coefficient of the antenna in presence of a metallic ground plane. The main telecom bands are highlighted: GSM-900 (*purple*), DCS-1800 and IMT-2000 (*green*), ISM2400 and LTE (*yellow*), WiMAX (*blue*)

**Fig. 2.18** Measured reflection coefficient (a) and corresponding reflection loss (b) of the antenna in presence of a hand with different grips. The main telecom bands are highlighted: GSM-900 (purple), DCS-1800 and IMT-2000 (green), ISM2400 and LTE (yellow), WiMAX (blue)



in practice,  $\Pi$ - and T-structured matching networks are commonly used in the tunable RF front-end.

The Tunable Matching Network (TMN) is based on a Pi-network composed of a fixed external inductor and two high power tunable capacitors integrated in a SOI CMOS 130 nm process. SOI CMOS provides an attractive trade-off among performance, cost and integration capability. Compared to standard bulk CMOS process, SOI CMOS features higher speed and reduced power consumption since the drain/source capacitances are substantially reduced. Moreover, the use of a high resistivity substrate enables high-Q integrated inductors, as well as excellent crosstalk isolation. Besides, by exploiting transistor stacking, SOI CMOS RF switch can be designed to handle arbitrarily high off-state voltages, which is a crucial feature for the implementation of a high power tunable matching network. Despite a higher wafer cost compared to standard bulk CMOS, the net impact of substrate cost on a fully packaged integrated circuit is quite small, and it is believed to further decrease in the near future, eventually reaching parity with standard bulk CMOS.

Implementation of the tunable capacitors is based on banks of binary weighted switched capacitors, where floating body NMOS transistors are used as low loss

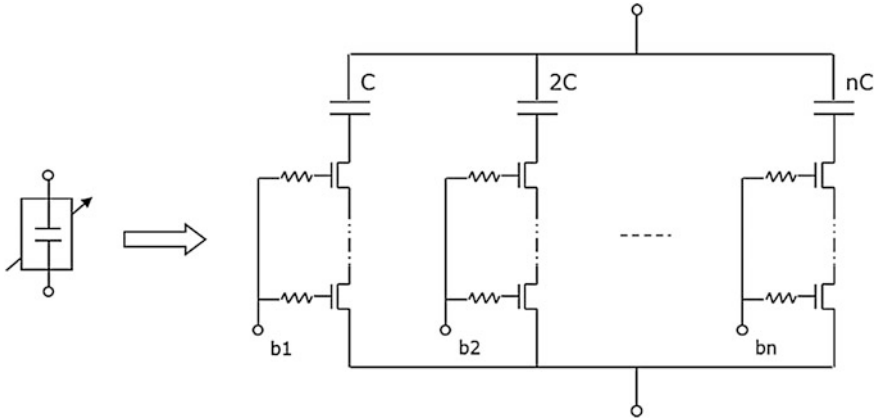


**Fig. 2.19** Implementation of a tuneable capacitor in SOI CMOS

switches to select the appropriate capacitance value. As shown in Fig. 2.19, multiple transistors have been stacked in series to prevent breakdown in OFF state by providing voltage division of the high power RF signal.

Each switched-capacitor exhibits 32 states and has been designed to cover the range 0.7–2.8 pF with a minimum quality factor of 40 at 2.7 GHz and a maximum power rating of 36 dBm. The size of the chip including two tunable capacitors, a negative bias generator and a Serial Peripheral Interface (SPI) is 1 mm<sup>2</sup>, and the power consumption is <1 mA under 2.5 V.

The chip has been directly attached on a dedicated FR4 test board as shown in Fig. 2.20. The external inductor is a surface mount device (SMD) from Johansson Technology and it has been soldered on the bottom layer of the test board.

A VHDCI connector is used to control the TMN which requires two analog inputs (VDD, PDN) for bias and three digital inputs (DCLK, DIN, DLOAD) for capacitors settings. Figure 2.21 shows the test setup used for small-signal characterization of the TMN, where a PXI module (not shown) is used to drive the SPI interface. A graphical user interface (GUI) has been developed under Labview to control the different instruments and allow acquisitions of S parameters of the TMN for different frequencies and capacitor states.

The TMN has been characterized experimentally in the frequency range of interest (1.7–2.7 GHz). The following figures show the measured smith chart coverage obtained for different inductance values, where the Smith chart coverage corresponds to the antenna impedance locus that can be matched to 50  $\Omega$  at TMN input (Fig. 2.22).

The TMN provides good impedance coverage at 2.2 and 2.7 GHz and is well centered on 50 Ohm at 2.2 GHz. At 1.7 GHz, impedance coverage is a bit limited and needs to be improved by further tuning of the inductor value or eventually by modifying the TMN configuration. Besides, the input impedance of the miniature dual-band antenna has to be checked to lie in the Smith chart coverage of the TMN.

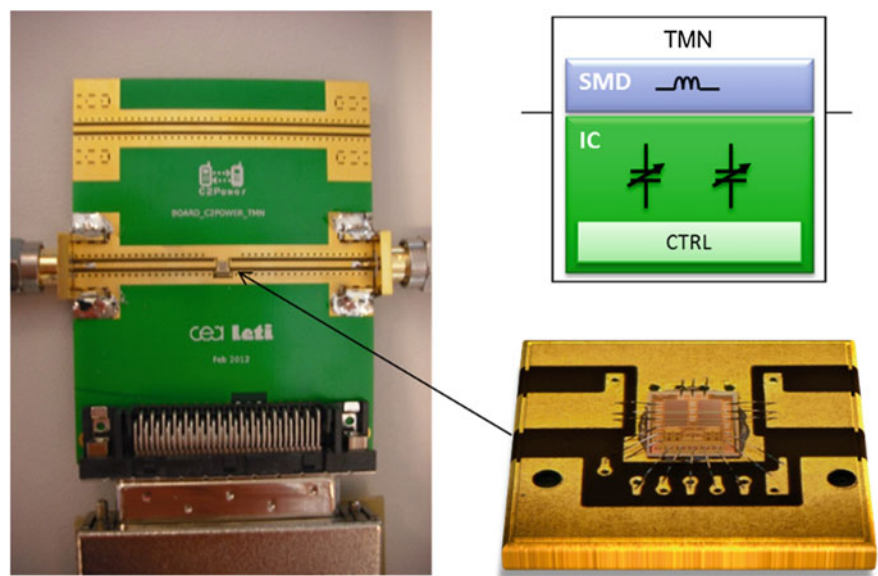


Fig. 2.20 Pictograph of the test board and tunable capacitors IC

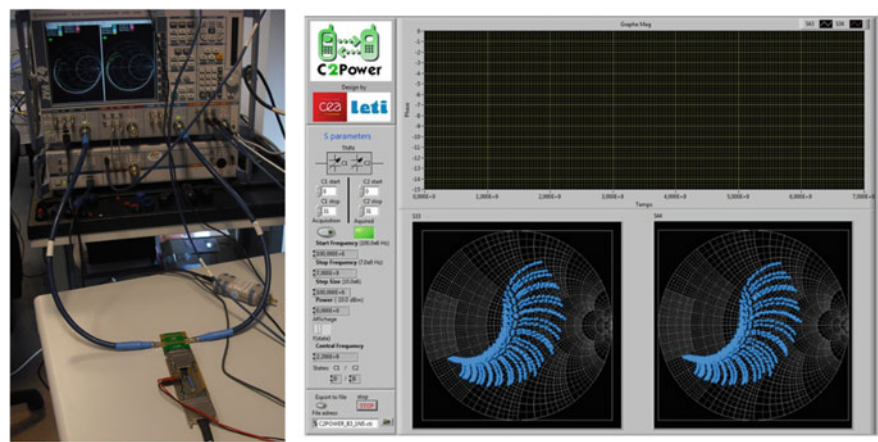
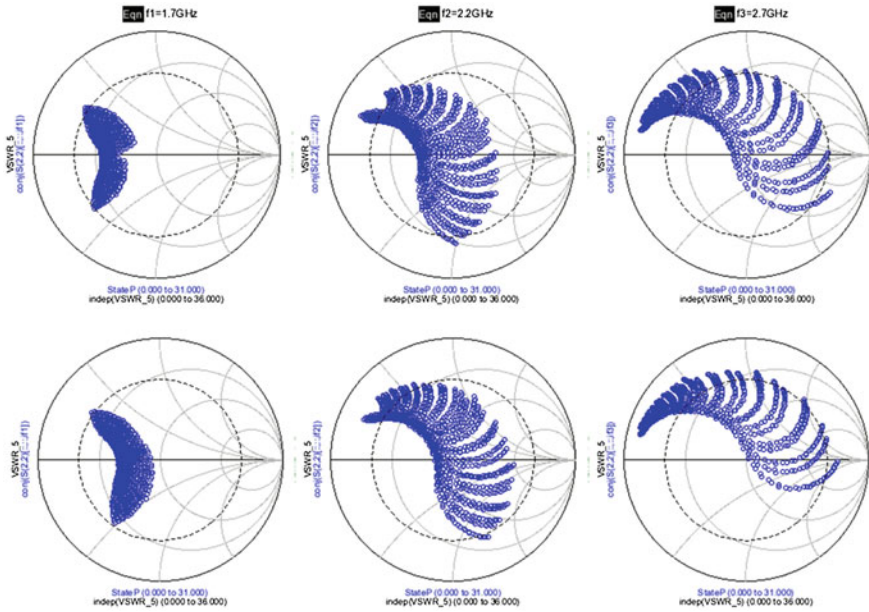


Fig. 2.21 Pictograph of the test setup (left) and TMN control user interface (right)

As shown in Figs. 2.23 and 2.24, a relatively good agreement is obtained between measurement and simulation for the 1,024 states of the TMN and in a large frequency range, including the band of interest.

At 2.2 and 2.7 GHz, a small shift between measurement and simulation can be observed and is partly due to higher losses than expected.



**Fig. 2.22** Measured Smith chart coverage for  $L = 1$  nH (*top*) and 1.5 nH (*bottom*) at 1.7, 2.2, and 2.7 GHz

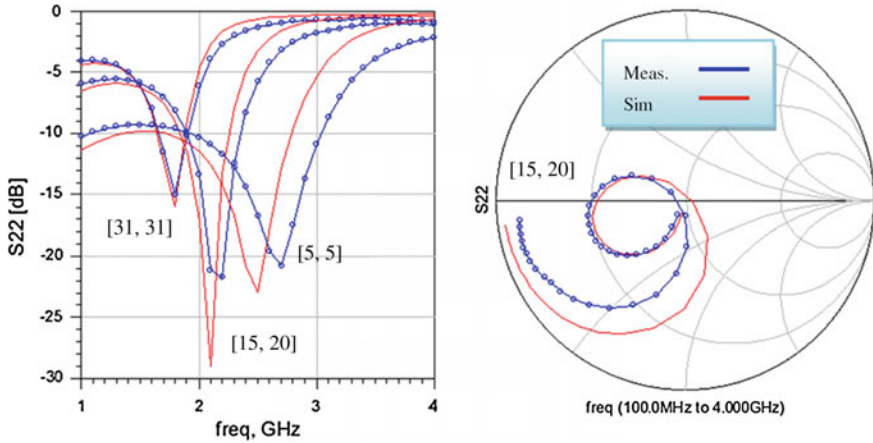


**Fig. 2.23** Measured and simulated  $S_{22}$  for different TMN states (*left*) and frequencies (*right*)

### 2.3.3 Mismatch Sensing Unit

The schematic and a photograph of the TMN-Antenna module are presented in Fig. 2.25. The main transmission branch is composed of the input selection switch, a couple, the TMN and the antenna. Two detectors measure the RF power in the



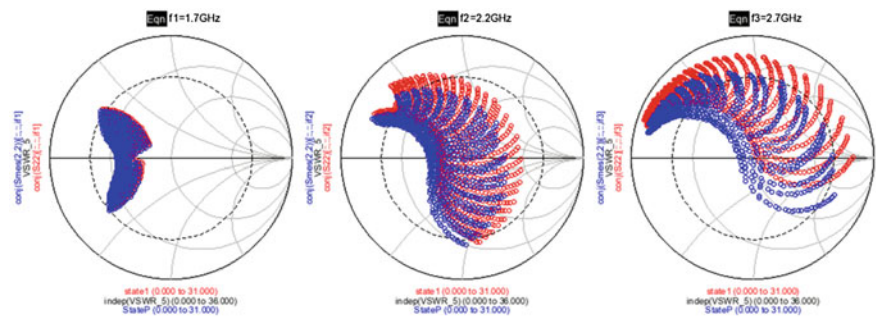


Fig. 2.24 Measured and simulated Smith chart coverage

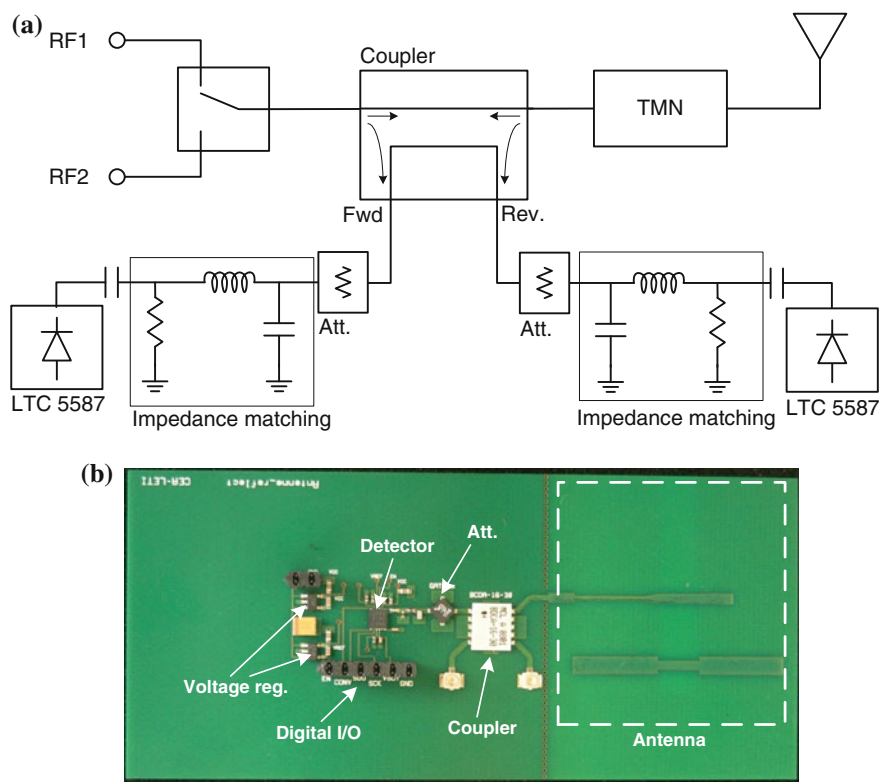


Fig. 2.25 **a** Schematic diagram of the TMN-Antenna module; **b** photograph of a preliminary prototype with a single detector and without the TMN

forward and reverse direction in order to compute the reflection coefficient. Each of these detectors is associated with an impedance matching network optimized for the 1.8–3.6 GHz band, as well as attenuators to adjust the input power to their dynamic range. The main components performances are described hereafter.



**Table 2.1** Main performances of the input selection switch Hittite HMC544

Insertion loss	0.4 dB @ 2 GHz 0.6 dB @ 3.5 GHz	Input power for 1 dB compression point	36 dBm with 3 V control 39 dBm for 5 V control
Isolation	>13 dB	Control	0/+ 3 V or 0/+ 5 V < 2 $\mu$ A

Switch Hittite HMC544 was chosen for its low insertion losses, high compression-point (it has to handle at least 1 W), and low power consumption. The main characteristics are summarized in Table 2.1.

The coupler is a Mini-Circuit BCDA-16-30+, which covers the 1,800–4,200 MHz band with about 16 dB coupling. Its insertion losses are typically 0.5 dB at 1,800–2,500 MHz and 0.7 dB at 3.5 GHz. Its directivity is typically 22 dB (Fig. 2.26).

The attenuator is from the GAT-xx+ series from Mini-Circuit and covers the DC-8 GHz band.

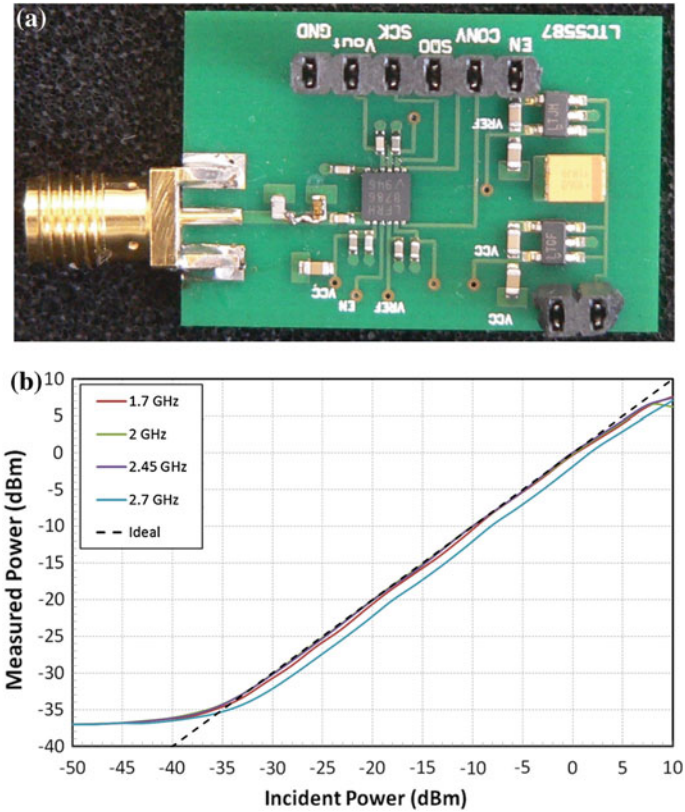


**Fig. 2.26** a Photo of the detector test board; b measured response of the detector

Detector LTC5587 from Linear Technology is a 10 MHz to 6 GHz low-power precision RMS power detector with an integrated 12-bit serial analog-to-digital converter. Its detection range is  $-34$  dBm to  $+6$  dBm. Its control requires three digital inputs (EN, CONV, SCK) and the output is delivered through a single digital output (SDO). It is a low-power component (3 mA at 3.3 V and 500 kcps). The maximum sampling frequency is 500 kcps. The detector was tested with an optimized matching network for the frequency band 1.7–2.7 GHz.

In order to validate the capabilities of the coupler and detectors to measure accurately the reflection coefficient, we simulated the antenna associated to the coupler and the detectors, and calculated the reflection coefficient from the detectors outputs. The coupler and detectors S-parameters are given by the manufacturer; the S parameter of the antenna was measured in different cases: antenna in free space, antenna perturbed by a ground plane at different distances, antenna perturbed by a hand. In each antenna case, the actual measured reflection coefficient of the antenna ( $\Gamma_{\text{meas}}$ ) was compared to the reflection coefficient calculated from the detectors outputs ( $\Gamma_{\text{detect}}$ ) over the frequency band 1.7–2.7 GHz. Figure 2.27b shows the error ( $\Gamma_{\text{detect}} - \Gamma_{\text{meas}}$ ) as a function of the actual reflection coefficient ( $\Gamma_{\text{meas}}$ ). We can observe that the error is limited to  $\pm 2$  dB, when the reflection coefficient is above  $-8$  dB, which is the domain where the TMN and therefore accurate measurements of the reflected power are needed. At low reflection coefficient levels ( $\Gamma_{\text{meas}} < -8$  dB), the errors are larger, which is expected since the power levels become close to the sensitivity of the detectors, but these errors are of no consequence since our goal is to know that the reflection level is below a certain level ( $\Gamma_{\text{meas}} < -9.5$  dB (VSWR  $< 2:1$ ) for instance) and not to have an accurate measurement.

### 2.3.4 Evaluation of the TMN-Antenna Performance

The TMN circuit simulations of the system have been performed to evaluate the expected performances. The simulation model takes into account the switched capacitors model, the series off-chip inductor, the interconnection parasitics (wirebonds) and the antenna.

The experimental antenna performances (impedance, efficiency) were introduced in the simulation in order to compute the actual radiated power taking into account the impedance mismatch loss and the losses of the antenna. To this purpose, the antenna is modeled as a 2-port component with the impedance of the antenna in port 1 and the effective transmission coefficient between port 1 and port 2. This transmission coefficient takes into account the reflection losses and an average efficiency of 70 % of the antenna.

Three typical cases are considered with respect to the antenna performances, corresponding to a favorable case and two critical cases:

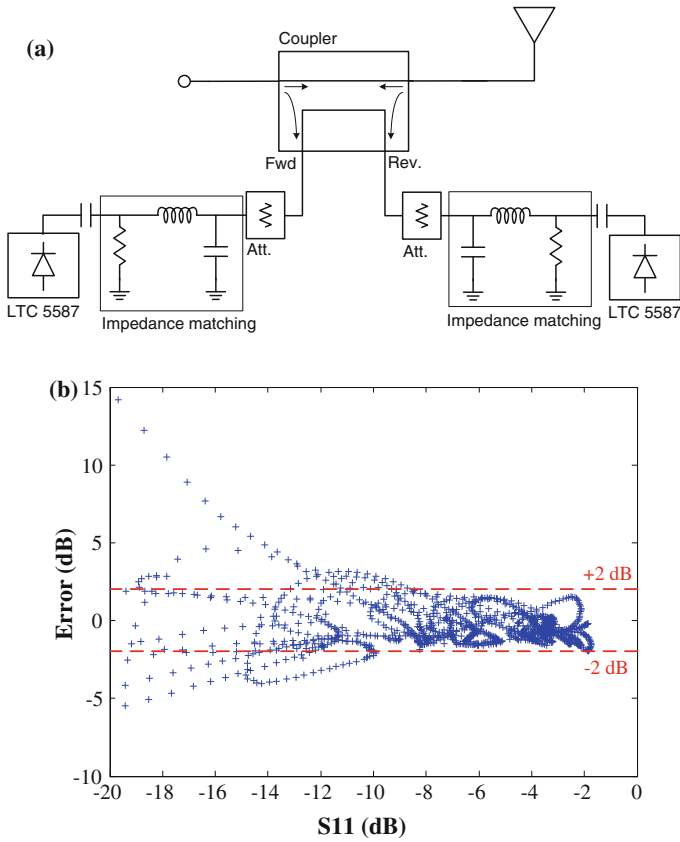


**Fig. 2.27** **a** Schematic of the antenna associated to the coupler and detectors; **b** simulation of the error between the reflection coefficient calculated from the detectors output and the actual reflection coefficient

- Case 1: Antenna in free space;
- Case 2: Antenna at 3 mm of a metal plane;
- Case 3: Antenna in hand (A heavily perturbed position).

The simulations reported here are performed at three frequencies (1.7, 2.2 and 2.7 GHz) representative of the targeted frequency band. A series inductance value of 2.2 nH was used here, although this value is subject to future optimization. For each antenna case, the optimal TMN state (out of 1,024 possible states) was selected for highest radiated power. The results are reported in the following subsections. A schematic representation of the simulation setup of the TMN-Antenna is represented by Fig. 2.28.

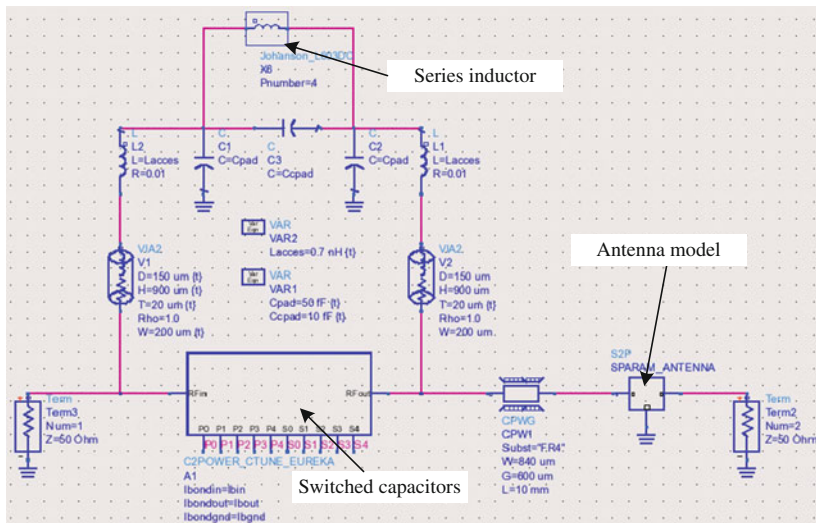


Fig. 2.28 Simulation schematic of the TMN-Antenna

### 2.3.4.1 Case 1: Antenna in Free Space

This is a favorable case since the antenna is unperturbed and therefore reasonably matched without TMN ( $S_{11} < -6.3$  dB). Figure 2.29 and Table 2.2 report the simulation results. At 1.7 and 2.2 GHz, the reflection coefficient is strongly improved to  $-32$  and  $-25.8$  dB respectively. However, since there was no significant reflection loss to compensate, the final radiated power level is slightly degraded by 0.2–0.3 dB due to the insertion losses of the TMN. It is seen from the figure that TMN states are available with a VSWR  $< 1.5:1$  at these two frequencies.

At 2.7 GHz, the TMN states are actually concentrated outside of the circle VSWR = 5:1, and the performances are here severely degraded with a reduction of the radiated power level by 3 dB. In this latter case, it is seen that the TMN is

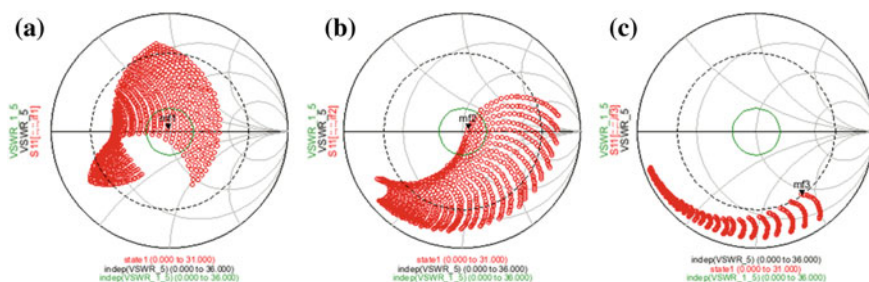


Fig. 2.29 Simulation of the 1,024 impedance states of the TMN-Antenna module in case 1 at **a** 1.7 GHz, **b** 2.2 GHz, and **c** 2.7 GHz

**Table 2.2** Performance summary of the TMN-Antenna module in case 1

	1.7 GHz				2.2 GHz				2.7 GHz			
	State #		Performance (dB)		State #		Performance (dB)		State #		Performance (dB)	
	C1	C2	S <sub>11</sub>	S <sub>21</sub>	C1	C2	S <sub>11</sub>	S <sub>21</sub>	C1	C2	S <sub>11</sub>	S <sub>21</sub>
No TMN	–	–	–6.3	–2.7	–	–	–11.1	–1.9	–	–	–12.4	–1.8
TMN	28	21	–32.1	–3.0	0	4	–25.8	–2.1	0	0	–3.6	–4.8
Gain	–	–	–	–0.3	–	–	–	–0.2	–	–	–	–3.0

detrimental to the performances of the system and therefore needs to be optimized. The main optimization parameters are the series inductor and the transmission line length between the TMN and the antenna.

2.3.4.2 Case 2: Antenna at 3 mm of a Metal Plane

This case is one of the most critical cases considered with reflection coefficients as high as –1.6 dB.

Figure 2.30 and Table 2.3 report the simulation results. At the three frequencies, the reflection coefficient is strongly improved to below –11 dB. In turn, the radiated power is improved by 1 and 2.4 dB respectively at 1.7 and 2.2 GHz. At 2.7 GHz, the insertion losses of the TMN compensate the reflection loss reduction so that there is no net benefit.

2.3.4.3 Case 3: Antenna in Hand

We evaluated several hand positions to assess the influence of the user’s hand on the antenna. One of the most critical was the hand position, where the user’s finger touches the antenna slot, resulting in a reflection coefficient in the range –3 to –4 dB. Figure 2.31a shows a CAD view of the specific hand position.

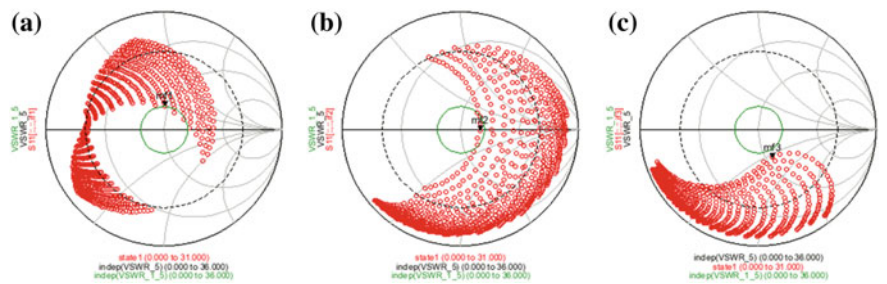


**Fig. 2.30** Simulation of the 1,024 impedance states of the TMN-Antenna module in case 2 at **a** 1.7 GHz, **b** 2.2 GHz, and **c** 2.7 GHz

**Table 2.3** Performance summary of the TMN-Antenna module in case 2

	1.7 GHz				2.2 GHz				2.7 GHz			
	State #		Performance (dB)		State #		Performance (dB)		State #		Performance (dB)	
	C1	C2	S <sub>11</sub>	S <sub>21</sub>	C1	C2	S <sub>11</sub>	S <sub>21</sub>	C1	C2	S <sub>11</sub>	S <sub>21</sub>
No TMN	–	–	–2.4	5.3	–	–	–1.6	–6.6	–	–	–7.2	–2.5
TMN	31	24	–14.1	4.3	18	0	15.7	–4.2	0	1	–11.4	–2.5
Gain	–	–	–	+1.0	–	–	–	+2.4	–	–	–	0.0

Figure 2.31 and Table 2.4 report the simulation results. At 1.7 and 2.7 GHz, the reflection coefficient is strongly improved to below  $-16$  dB. In turn, the radiated power is improved by 1 and 1.5 dB respectively. Figure 2.31 shows that several

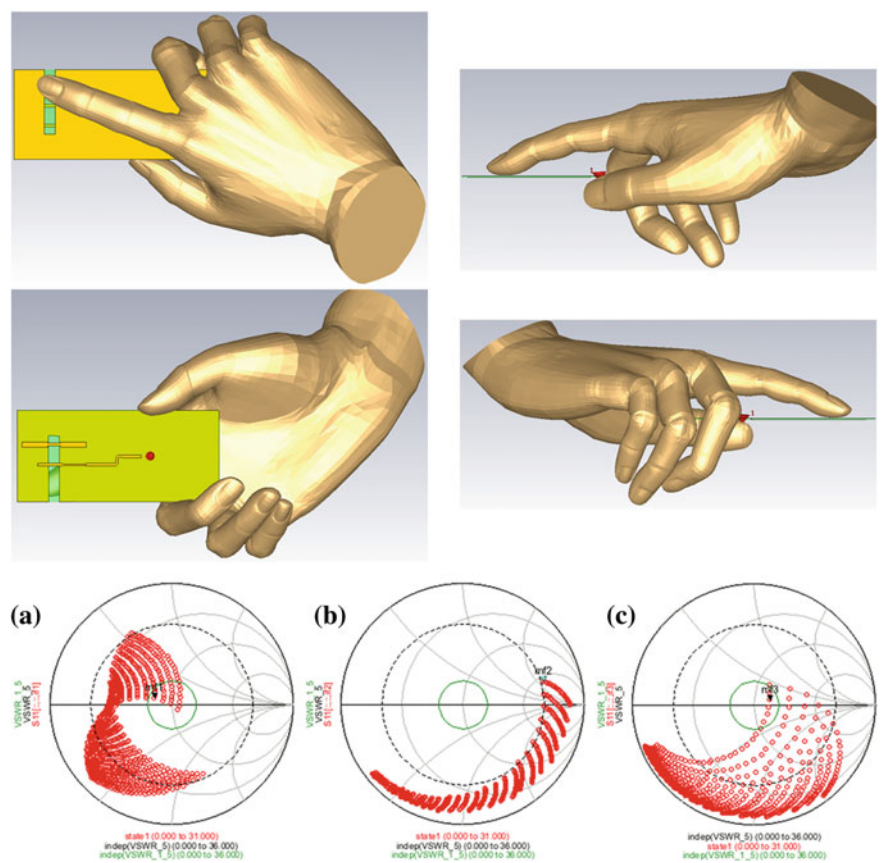


**Fig. 2.31** CAD views of the Hand#2 position (case 3) and simulation of the 1,024 impedance states of the TMN-Antenna module at **a** 1.7 GHz, **b** 2.2 GHz, and **c** 2.7 GHz

**Table 2.4** Performance summary of the TMN-Antenna module in case 3

	1.7 GHz				2.2 GHz				2.7 GHz			
	State #		Performance (dB)		State #		Performance (dB)		State #		Performance (dB)	
	C1	C2	S <sub>11</sub>	S <sub>21</sub>	C1	C2	S <sub>11</sub>	S <sub>21</sub>	C1	C2	S <sub>11</sub>	S <sub>21</sub>
No TMN	–	–	–3.1	–4.4	–	–	–3.8	–3.9	–	–	–3.4	–4.2
TMN	31	28	–16.5	–3.4	0	0	–3.3	–5.5	2	0	–17.3	–2.7
Gain	–	–	–	+1.0	–	–	–	–1.6	–	–	–	+1.5

impedance states are well into the  $VSWR = 1.5$  circle. At 2.2 GHz, there is no impedance state in the  $VSWR = 5$  circle; the reflection coefficient is slightly degraded and the transmission coefficient is reduced by 1.6 dB due to the insertion losses of the TMN. A further investigation based on a larger set of hand positions and test frequencies will lead to a better assessment of the occurrence of this issue, i.e. to determine if there is an actual weakness of the design at 2.2 GHz or if there are rare cases like this one. Nevertheless, considering the randomness and wide range of antenna perturbation occurring in actual applications, it is not expected to reach a net benefit in all the cases and all the frequencies. The design optimization may be done at the level of the series inductance (which can be easily changed) or the switched capacitors (which would require another CMOS fabrication runs).

The three antenna cases presented above show promising performances and lead to the following main conclusions:

- When the antenna is correctly matched, the TMN slightly degrade the overall efficiency of the system due to its own insertion losses [34, 35]. This is why it is of upmost importance to design such circuits in advanced technologies with minimum losses such as CMOS-SOI, RF MEMS, or Silicon on-Sapphire. This degradation can be acceptable if limited to about 0.5 dB on average, which is the case here at least in the range 1.7–2.2 GHz (Table 2.2).
- In critical configurations such as cases 2 and 3 presented above, the TMN can result in an improvement of the radiated power by 1–2.4 dB, which corresponds to an efficiency improvement of 25–73 %.
- In some cases of antenna configuration and frequency, the TMN does not provide an acceptable matching state. This can be improved by (i) further optimization of the inductance/capacitance values, (ii) reducing the targeted bandwidth to achieve a better optimization, (iii) increasing the number of states at the cost of increased complexity.

It is important to note that another factor of improvement not evaluated here is the benefit for the power amplifier efficiency of the better output impedance matching achieved thanks to the TMN in an integrated terminal. This topic is beyond the scope of this work, since it would require a co-design and close integration of the power amplifier and TMN.

## 2.4 Conclusion

This chapter presents a design approach for the RF front-end in multi-mode future emerging handsets, and engineered according towards energy saving, miniaturization, flexibility and re-configurability. The chapter mainly addresses two topics: the design of a multi-standard transceiver and the design of energy efficient miniature antennae co-designed with a matching network to overcome the perturbation caused by user's hand, face or metal close to the antenna.

At the transceiver level, a major challenge is to implement integrated architectures addressing multiple standards in different bands with a minimum of off-chip components for better miniaturization and lower energy consumption. We provided a generic design for a multi-standard RF transmitter architecture, with specific use-cases for TETRA, TETRAPOL and LTE. The performance results show the feasibility of innovative architectures with a high level of integration in state-of-the-art silicon CMOS technologies.

Pivotal to the RF front end in mobile handset, is the requirement for miniature antennae. We presented investigated candidate energy efficient design along with a matching network, to study the perturbation by and sensitivity of miniature antenna to metal sheets, user's hand or the human head. The miniature antennae embedded into wireless terminals are quite sensitive to their environment and exhibit wide impedance variations, resulting in high reflection losses between the RF front-end and the antenna. The antenna has been designed and demonstrated with an excellent agreement between the simulations and the measurements. It covers the GSM band as well as the 1.7–3.6 GHz band with a reflection coefficient better than  $-6$  dB and efficiency higher than 70 %. The sensitivity of this antenna to its environment was investigated and it was found that the presence of a metallic plane or the user's hand close to the antenna would lead to reflection coefficients as high as  $-2$  dB, which corresponds to  $-4.3$  dB of losses.

The tunable matching network is based on a CLC pi-network with switched capacitors fabricated in CMOS-SOI technology. This circuit has been designed for the 1.7–2.7 GHz band.

A sensing unit was designed based on an integrated coupler and two power detectors measuring the incident and reflected power levels. This circuit was tested and operates adequately over the 1.7–2.7 GHz band with a good accuracy. An advantage of this implementation is the very low power consumption of the detectors ( $<10$  mW). A drawback is that only the magnitude of the reflection coefficient is measured. Other sensing systems reported in the literature allow the measurement of the complex impedance using power and phase measurements. The power consumption of the TMN-Antenna module is quite low; it is estimated at  $<30$  mW (10 mW per detector, 2.5 mW for the TMN). Finally, the performance of the TMN-Antenna module was evaluated by simulations in several cases of antennae with or without perturbation. The results indicate an efficiency improvement of more than 25 % in cases of strong perturbations.



It is worth noting that the insertion losses of the TMN always result in some performance reduction in specific cases where the antenna is not perturbed, which is expected due to the adding of circuits [34, 35]. On the other hand, it provides great benefits in cases of strong perturbations. Therefore, an accurate evaluation of its benefit to the overall power consumption of the terminal would require a statistical investigation of the terminal usage to determine the long-term average gain. To the best of the author's knowledge, such investigation has never been realized but it is interesting to note the recent announcements of leading terminal manufacturers of the integration of TMN systems in their terminals.

## References

1. Wong, A., Kathiresan, G., Chan, C., et al.: A 1 V wireless transceiver for an ultra-low-power SoC for biotelemetry applications. *IEEE J. Solid-State Circuits* **43**(7), 1511 (2008)
2. Quinlan, P., Crowley, P., Chanca, M., et al.: A multimode 0.3–200-kb/s transceiver for the 433/868/915-MHz bands in 0.25- $\mu$ m CMOS. *IEEE J. Solid-State Circuits* **39**(12), 2297 (2004)
3. Qi, Z., Kuang, X., Wu, N.: An ultra-low-power RF transceiver for WBANs in medical applications. *J. Semiconductors* **32**(6), 065008 (2011)
4. Peiris, V., Arm, C., Bories, S., et al.: A 1 V 433/868 MHz 25 kb/s-FSK 2 kb/s-OOK RF transceiver SoC in standard digital 0.18  $\mu$ m CMOS. *IEEE ISSCC Digest of Technical Papers*, vol. 48, p. 258 (2005)
5. Guofeng, L., Nanjian, W.: A low power flexible PGA for software defined radio systems. *J. Semiconductors* **33**(5), 055006 (2012)
6. Telecommunications Industry Association: APCO Project 25 System and Standards Definition. Telecommunications Industry Association, Arlington, TIA/EIA-102.A (1995)
7. Telecommunications Industry Association: Project 25 FDMA Common Air Interface New Technology Standards Project Digital Radio Technical Standards. Telecommunications Industry Association, Arlington, TIA/EIA-102.BAAA (1998)
8. Cayla, G.: TETRA: the new digital professional mobile radio. In: *Proceedings of 5th Seminar on Digital Mobile Radio Communications*, pp. 113–118 (1992)
9. <http://www.tetrapol.com/>
10. Skrivervik, A.K., Zurcher, J.-F., Staub, O., Mosig, J.R.: PCS antenna design: the challenge of miniaturization. *IEEE Antennas Propag. Mag.* **43**, 12–27 (2001)
11. Lee, C.S., Tseng, K.-H.: Size reduction of microstrip antennas. *Electron. Lett.* **37**, 1274–1275 (2001)
12. Shackelford, A.K., Lee, K.F., Luck, K.M.: Design of small-size wide bandwidth Microstrip patch antennas. *IEEE Antennas Propag. Mag.* **45**, 75–83 (2003)
13. Deshmukh, A.A., Kumar, G.: Half U-slot loaded rectangular microstrip antenna. In: *IEEE Antennas Propagation Society International Symposium*, vol. 2, pp. 876–879, Columbus OH (2003)
14. Chair, R., Mak, C.-L., Lee, K.-F., Luk, K.-M., Kishk, A.A.: Miniature wide-band half U-slot and half E-shaped patch antennas. *IEEE Trans. Antennas Propagat.* **53**, 2645–2651 (2008)
15. Guo, L., Wang, S., Chen, X., Parini, C.: Miniaturised antennas for UWB communications. In: *Proceedings of the European Conference on Antennas and Propagation*, pp. 3774–3778. Berlin, Germany, 23–27 Mar 2009
16. Gianvittorio, J.P., Rahmat-Samii, Y.: Fractal antennas: a novel antenna miniaturization technique, and applications. *IEEE Antennas Propag. Mag.* **44**(1), 20–36 (2002)

17. Byndas, A., Hossa, R., Bialkowski, M.E., Kabacik, P.: Investigation into operation of single and multi-layer configurations of planar inverted-F antenna. *IEEE Antenna Propag. Mag.* **49**(4), 22–33 (2007)
18. Razali, A.R., Bialkowski, M.E., Tsai, F.-C.E.: Multi-band planar inverted-F antenna with microstripline coupling to open-end ground slots. In: *Proceedings of Asia Pacific Microwave Conference*, pp. 2471–2474, Dec 2009
19. Razali, A.R., Bialkowski, M.E.: Coplanar inverted-F antenna with open-end ground slots for multi-band operation. *IEEE Antenna Wirel. Propag. Lett.* **8**, 1029–1032 (2009)
20. Hossa, R., Byndas, A., Bialkowski, M.E.: Improvement of compact terminal antenna performance by incorporating open-end slots in ground plane. *IEEE Microw. Wirel. Compon. Lett.* **14**(6), 283–285 (2004)
21. Alam, M.S., Islam, M.T., Misran, N.: A novel compact split ring slotted electromagnetic bandgap structure for microstrip patch antenna performance enhancement. *Prog Electromagnet. Res* **130**, 389–409 (2012)
22. Yu, A., Yang, F., Elsherbeni, A. Z.: A dual band circularly polarized ring antenna based on composite right and left handed metamaterial. *Prog Electromagnet. Res* **78**, 73–81 (2008)
23. Sayem, A.T.M., Ali, M.: Characteristics of a microstrip-fed miniature printed Hilbert slot antenna. *Prog Electromagnet. Res* **56**, 1–18, (2006)
24. Niamien, M.A.C., Dussopt, L., Delaveaud, C.: A Compact dual-band notch antenna for wireless multi-standard terminals. *IEEE Antennas Wirel. Propag. Lett.* **11**, 877–880 (2012)
25. Karimullah, K., Nyquist, D., Chen, K.: Interaction of thin wire antennas with conducting, polarizable bodies—theory and experiment. In: *Proceedings of IEEE International Symposium on Antennas and Propagation Society (APS '78)*, vol. 16, pp. 219–222. College Park, Md, USA, May 1978
26. Norklit, O., Teal, P.D., Vaughan, R.G.: Measurement and evaluation of multi-antenna handsets in indoor mobile communication. *IEEE Trans. Antennas Propag.* **49**(3), 429–437 (2001)
27. Jensen, M.A., Rahmat-Samii, Y.: Performance analysis of antennas for hand-held transceivers using FDTD. *IEEE Trans. Antennas Propag.* **42**(8), 1106–1113 (1994)
28. Toftgard, J., Hornsleth, S.N., Andersen, J.B.: Effects on portable antennas of the presence of a person. *IEEE Trans. Antennas Propag.* **41**(6), 739–746 (1993)
29. de Mingo, J., Valdovinos, A., Crespo, A., Navarro, D., Garcia, P.: An RF electronically controlled impedance tuning network design and its application to an antenna input impedance automatic matching system. *IEEE Trans. Microw. Theory Tech.* **52**(2), 489–497 (2004)
30. Vicki Chen, L.-Y., Forse, R., Chase, D., York, R. A.: Analogtunable matching network using integrated thin-film BST capacitors. In: *IEEE MTT-S International Microwave Symposium Digest*, vol. 1, pp. 261–264. FortWorth, Tex, USA, June 2004
31. Moritz, J.R., Sun, Y.: Frequency agile antenna tuning and matching. In: *Proceedings of 8th International Conference on HF Radio Systems and Techniques (IEE Conf. Publ. No. 474)*, pp. 169–174. Guildford, UK, July 2000
32. Leenaerts, D.M.W.: Low power RF IC design for wireless communication. In: *Proceedings of International Symposium on Low Power Electronics and Design*, pp. 428–433. Seoul, Korea, Aug 2003
33. Abidi, A.A.: Low-power radio-frequency IC's for portable communications. *Proc. IEEE* **83**(4), 544–569 (1995)
34. Van Bezooijen, A.: Antenna tuner for hand-sets. In: *Proceedings of Advancements in Front End Modules for Mobile and Wireless Applications workshop*, 2012 IEEE MTT-S Int. Microwave Symposium, June 2012
35. Boyle, K.R., Spits, E., de Jongh, M.A., Sato, S., Bakker, T., Van Bezooijen, A.: A self-contained adaptive antenna tuner for mobile phones. In: *Proceedings of 6th European Conference on Antennas and Propagation (EuCAP 2012)*, pp. 1804–1808, Mar 2012

Energy Efficient Smart Phones for 5G Networks

Radwan, A.; Rodriguez, J. (Eds.)

2015, XIII, 267 p. 170 illus., 132 illus. in color.,

Hardcover

ISBN: 978-3-319-10313-6